Rapid Imaging of Tumor Cell Death *in vivo* using the C2A domain of Synaptotagmin-I

André A. Neves[1][*], Bangwen Xie[1], Sarah Fawcett[1], Israt S. Alam[1], Timothy H. Witney[2], Maaike M. de Backer[2], Julia Summers[1], William Hughes[1], Sarah McGuire[1], Dmitry Soloviev[1], Jodi Miller[1], William J. Howat[1], De-en Hu[1], Tiago B. Rodrigues[1], David Y. Lewis,[1] and Kevin M. Brindle[1,2]

[1]Cancer Research UK Cambridge Institute, Li Ka Shing Centre, Robinson Way, Cambridge CB2 0RE, UK, [2]Department of Biochemistry, University of Cambridge, Tennis Court Road, Cambridge CB2 1GA, UK.

*Corresponding author: André A. Neves, CRUK Cambridge Institute, Li Ka Shing Centre, Robinson Way, Cambridge CB2 0RE, UK. Tel. +44 (0)1223 769518, Fax +44 (0)1223 766002, Email: andre.neves@cruk.cam.ac.uk

Running title: Rapid Imaging of Tumor Cell Death

1

Cell death is an important target for imaging the early response of tumors to treatment. We describe here validation of a phosphatidylserine-binding agent for detecting tumor cell death *in vivo* based on the C2A domain of Synaptotagmin-I. **Methods:** The capability of near infrared fluorophore-labeled and ^{99m}Technetium- and ^{111}Indium-labeled derivatives of C2Am for imaging tumor cell death, using planar near infrared fluorescence (NIRF) imaging and single photon computed tomography (SPECT) respectively, was evaluated in implanted and genetically engineered mouse models of lymphoma and in a human colorectal xenograft. **Results:** The fluorophore labeled C2Am derivative showed predominantly renal clearance and high specificity and sensitivity for detecting low levels of tumor cell death (2-5%). There was a significant correlation (R>0.9, P<0.05) between fluorescently-labeled C2Am binding and histological markers of cell death, including cleaved caspase-3, whereas there was no such correlation with a site-directed mutant of C2Am (iC2Am) that does not bind phosphatidylserine. ^{99m}Tc-C2Am and ^{111}In-C2Am also showed favorable biodistribution profiles, with predominantly renal clearance and low non-specific retention in liver and spleen at 24 h after probe administration. ^{99m}Tc-C2Am and ^{111}In-C2Am generated tumor-to-muscle ratios in drug-treated tumors of 4.3× and 2.2× respectively at two hours and 7.3× and 4.1× respectively at twenty-four hours after administration. **Conclusions:** Given the favorable biodistribution profile of ^{99m}Tc- and ^{111}In-labelled C2Am, and their ability to produce rapid and cell death-specific image contrast, these agents have potential for clinical translation.

Detection of the early responses of tumors to therapy would allow rapid selection of the most effective treatment. Currently, clinical assessment of treatment response is based on Response Evaluation Criteria in Solid Tumors (RECIST), which define partial response as a reduction of at least 30% in the sum of the diameters of the target lesion (*1*). The problem for early detection of response is that these morphological changes may only occur weeks after the start of treatment and fail to detect response to cytostatic therapies (*2*).

Cell death is an important target for imaging early treatment response (*3*), since most treatments induce tumor apoptosis and/or necrosis. However, there is as yet no reliable technique for routine imaging of cell death in the clinic (*4*). Phosphatidylserine, which is externalized on the outer leaflet of the plasma membrane bilayer in apoptosis, and is exposed through permeabilization of the plasma membrane in necrotic cells, can be detected using the 36-kDa phosphatidylserine–binding protein, Annexin-V (AnxV) (*5*). [99mTc]-labeled AnxV has been used to image drug-induced cell death in human tumors, including breast, lymphoma, lung (*6*) and head and neck squamous cell carcinoma (*7*). However, despite early promise, and the development of novel site-directed mutants of AnxV with improved biodistribution (*8*), problems with this agent persisted (*9*), including suboptimal pharmacokinetics and non-specific binding (*10*).

We have developed a phosphatidylserine-targeted agent based on the C2A domain of Synaptotagmin-I. This was first used, in animal models, in the form of a dimeric glutathione S-transferase (GST)-tagged construct (84 kDa) for imaging tumor cell death using MRI (*11,12*) and, in [99mTc]-labeled form, for imaging tumor cell death (*13*) and cardiac ischemia using SPECT (*14*), and, in [18F]-labeled form, for imaging cell death in a rabbit lung cancer model using PET (*15*).

More recently, we have used the isolated C2A domain, (*16*), which is much smaller (16 kDa), giving better tissue access and clearance, in which we have introduced a site-directed mutation (S78C; C2Am) that allows site-specific modification with an imaging label. Studies *in vitro* demonstrated that this probe showed a four-fold lower binding to viable cells and consequently improved specificity for detecting apoptosis and necrosis, when compared with AnxV (*16*). Moreover, removal of the GST tag, which is likely to be immunogenic, should facilitate translation of this agent to the clinic.

3

We have evaluated here the speed of detection, specificity, sensitivity and biodistribution profiles of AlexaFluor™750- and [99m]Tc- and ^{111}In-labeled C2Am, for NIRF and SPECT imaging, respectively, of cell death in implanted models of lymphoma (EL4) (*11*) and colorectal cancer (Colo-205) (*17*), and in a spontaneous Myc-driven model of Burkitt's lymphoma (Eμ-myc) (*18*). We also describe a site-directed mutant of C2Am (iC2Am, D108N) that is inactive in phosphatidylserine binding, which we used to demonstrate that there were only low levels of non-specific probe retention.

MATERIALS AND METHODS

Probe expression and chemical labeling

C2Am and iC2Am were expressed, purified and labeled using AlexaFluor™-750 C5-maleimide, maleimide-HYNIC (for ^{99m}Tc) and maleimide-DOTA (for ^{111}In) as described previously (*16*). Successful conjugation was confirmed using electrospray ionization mass spectrometry (ESI-MS) and radio HPLC (Supplemental Figs. 1-2). Phosphatidylserine binding activity of the conjugates was confirmed by surface plasmon resonance measurements (Supplemental Table 1).

Cell culture

EL4, murine lymphoma and Colo-205, human colorectal cells (ATCC) were cultured in RPMI medium (Life Technologies) containing 300 mg/L L-glutamine and 10% (v/v) fetal bovine serum (FBS, PAA Laboratories). Cell death was induced in EL4 cells by treatment with 15 µM etoposide (Pharmachemie BV) for 24 h at 37 °C. An automated analyzer (Vi-Cell™, Beckman Coulter) was used to monitor cell number and viability.

Animals and tumor models

EL4 or Colo-205 cells (>95% viability) were washed, re-suspended in chilled PBS, and implanted (5×10^6 cells) subcutaneously under isoflurane anesthesia, in the flank of C57BL/6 (BL6) or between the shoulder blades of BALB/c Nude (NU) mice (8-12 week old females, from Charles Rivers Laboratories) respectively. Tumors were allowed to

develop for between 8−13 days. Animals bearing EL4 tumors were treated with 67 mg/kg body weight etoposide (i.p.), or solvent vehicle, at 24 h prior to imaging. BALB/c Nude mice bearing Colo-205 tumors were treated with 250 mg/kg body weight 5-fluorouracil (Sigma-Aldrich, 5-FU; i.p.) or solvent vehicle, at 24 h prior to imaging. Eµ-myc animals (Jackson Laboratories) were monitored daily and enrolled into the study when palpable lymph node masses were detectable (18). The mice were treated with 200 mg/kg body weight cyclophosphamide (Sigma-Aldrich; i.p.) 24−48 h prior to imaging.

Biodistribution and NIRF imaging studies

C2Am-AF750, iC2Am-AF750 or AnxV-750 (Annexin-Vivo™, Perkin Elmer) were administered at 0.10 µmol/kg (10 mL/kg, i.v.) to tumor-bearing NU mice. Imaging *in vivo* and/or *ex vivo* was performed using Li-Cor Pearl-Impulse™ or Xenogen IVIS200™ (Perkin Elmer) small animal imaging systems. Li-Cor Imaging Studio software (version 3.1.4) or Perkin Elmer Living Image (version 3.2) were used for image analysis.

Biodistribution and SPECT studies

Twenty-four hours after chemotherapy treatment, tumor-bearing mice received an injection (10 mL/kg, i.v.) of either ^{99m}Tc–C2Am (EL4 and Eµ-myc models) or ^{111}In–C2Am (Colo-205 model) at 7.5 nmol/kg (0.12 mg/kg, or ca. 1.5-2 MBq per mouse). SPECT studies were conducted in separate cohorts of mice 2 h after administration of radiolabelled C2Am at 75 nmol/kg, i.v., 1.2 mg/kg or ca. 15-20 MBq per mouse. Specific activities were 10-11.5 MBq/nmol for both ^{99m}Tc- and ^{111}In-labeled C2Am. Injected doses were determined using a Dose Calibrator (ISO-MED 2000, MED Nuklear-Medizintechnik GmbH) and corrected for decay.

Study approval

All animal experiments were performed in compliance with a project license issued under the Animals (Scientific Procedures) Act of 1986 and were designed with reference to the UK Co-ordinating Committee on Cancer Research guidelines for the welfare of animals in experimental neoplasia (19). Protocols were approved by the Cancer Research UK, Cambridge Institute Animal Welfare and Ethical Review Body.

Additional information is available in *Supplemental Materials and Methods*.

RESULTS

Preparation and characterization of imaging probes

iC2Am-AF750 was produced by site-directed mutagenesis (D108N) of C2Am. This mutation abolishes binding to phosphatidylserine (*20*). C2Am and iC2Am were prepared and labeled with Alexa Fluor™-750 (C2Am-AF750, iC2Am-AF750), as described previously (*16*). The proteins were fully modified, yielding a single molecular species on ESI-MS (Supplemental Fig. 1A-B). C2Am-AF750, C2Am-HYNIC and C2Am-DOTA bound phosphatidylserine with similar affinities (Kd~60-90 nM; Supplemental Table 1), as determined using surface plasmon resonance measurements (*16*). As expected, iC2Am-AF750 showed no binding. C2Am was also modified stoichiometrically with maleimide-HYNIC or maleimide-DOTA, generating single species of MW 16426.5 Da, and 16749.8 Da, respectively, as determined by ESI-MS (Supplemental Fig. 1C-D). C2Am-HYNIC was loaded with ^{99m}Tc using methods described previously (*21*). C2Am-DOTA was loaded with ^{111}InCl$_3$ as described in Supplemental Methods. The conjugates were analyzed by HPLC (Supplemental Fig. 2). Radiolabeling efficiency was >94%.

Fluorescence imaging of tumor cell death *in vivo*

There was increased retention of C2Am-AF750 in drug-treated as compared to untreated EL4 (Fig. 1A, 2A), Colo-205 (Fig. 1B, 2B) and Eμ-myc tumors (Fig. 1C, 2C) at 24 h after probe injection. Anx-AF750 showed no increase in retention following drug treatment in any of the tumor models. Although Anx-AF750 fluorescence was greater than that of C2Am-AF750 in the EL4 tumor model this was not increased by drug treatment. The retention of iC2Am-AF750 in drug-treated tumors was less than of C2Am-AF750 in all of the tumor models and there was no significant difference in the retention of iC2Am-AF750 in untreated or treated Colo-205 (Fig. 2B) and Eμ-myc tumors (Fig. 2C). In drug-treated EL4 tumors there was an increase in tumor

6

fluorescence in animals injected with iC2Am-AF750 (Fig. 2A), however the levels were 3× lower than with C2Am-AF750. This may be due to a treatment-induced increase in the enhanced permeability and retention (EPR) effect in this tumor model (*22*). The heterogeneous skin pigmentation of Eµ-myc mice prevented accurate optical imaging *in vivo* and therefore for this tumor model fluorescence was measured *ex vivo* (Fig. 2C), which may explain the better contrast observed. All three tumor models showed a correlation between whole tumor mean C2Am-AF750 fluorescence intensities and CC3 staining of histological sections obtained *post mortem* (Fig. 2A-C, lower panels). This correlation was confirmed microscopically (Fig. 3). In Eµ-myc tumors C2Am-AF750 fluorescence was detected from regions where CC3 staining occupied as little as 1-2% of the ~1 mm^2 regions of interest (Fig. 3C). Differences in the relationship between fluorescence intensity and the levels of cleaved caspase-3 in the different tumors (Fig. 3) may reflect differences in phosphatidylserine exposure.

Cell binding experiments with ^{99m}Tc-C2Am

As we were unable to detect treatment response with AnxV-AF750, despite using the most recent agent and according to the manufacturer's instructions, radionuclide imaging studies were performed solely with C2Am labeled with either ^{99m}Tc or [111]In. There was a significant increase in the radioactivity retained by washed cell pellets prepared from suspensions of EL4 lymphoma cells that had been treated with etoposide (15 µM, for 24 h) and then incubated with ^{99m}Tc-C2Am in the concentration range of 1-100 nM (Fig. 4A). Cell viability decreased from 95% to 75% in these drug-treated cells, as assessed by trypan blue dye exclusion.

Biodistribution

[99m]Tc-C2Am and ^{111}In-C2Am showed favorable biodistribution profiles with predominantly renal clearance (Table 1). ^{99m}Tc-C2Am had blood half-lives in EL4 tumor-bearing animals of 7.2±0.6 h and 9.7±0.1 h in etoposide-treated and untreated animals, respectively. ^{111}In-C2Am showed similar half-lives in Colo-205 tumor-bearing animals of 11.4±1.2 h and 8.0±0.8 h in 5-FU-treated and untreated animals, respectively. Tumor-to-blood ratios increased progressively in chemotherapy-treated EL4 tumor-

bearing animals, from 1.71±0.40 at 2 h to 6.96±1.08 at 24 h for ^{99m}Tc-C2Am and from 1.38±0.65 at 2 h to 5.43±0.96 at 24 h for ^{111}In-C2Am in Colo-205 tumor-bearing animals. There was significantly greater retention in tumors and spleens (Fig. 4B, P<0.05) from etoposide-treated EL4 tumor-bearing animals, from as early as 2 h following drug administration. The spleens showed significant increases in the levels of cell death following drug treatment (Supplemental Fig. 3).

The biodistribution profiles of C2Am-AF750 and iC2Am-AF750 (Supplemental Table 2) were similar to those of ^{99m}Tc-C2Am and ^{111}In-C2Am (Table 1). As with ^{99m}Tc-C2Am and ^{111}In-C2Am, C2Am-AF750 generated EL4 tumor-to-muscle contrast from as early as 2 h (2.2±0.49) and up to 24 h (3.63±0.4) post injection of the imaging agent (Supplemental Table 2).

SPECT imaging of tumor cell death *in vivo* using ^{99m}Tc-C2Am and ^{111}In-C2Am

Images were acquired from animals with implanted Colo-205 (Fig. 5A) tumors and from tumor-bearing Eμ-myc mice (Fig. 6A) prior to and 24 h after treatment with 5-FU or cyclophosphamide, respectively, and 2 h after injection of ^{111}In-C2Am or ^{99m}Tc-C2Am, respectively. Corresponding studies with ^{99m}Tc-C2Am in etoposide-treated EL4 tumors are shown in Supplemental Fig. 4. Maximum activity was observed in the kidneys and bladder, consistent with a predominantly renal excretion route (Table 1). Renal retention was mostly cortical (see Supplemental Fig. 4A). In 5-FU-treated Colo-205 tumors (Fig. 5) ^{111}In-C2Am uptake was increased by ∼1.6× (Fig. 5B, upper panel, P<0.05), reflecting a similar increase (1.65×) in the percentage of dead cells determined histologically in tumor sections (Fig. 5B, lower panel, P<0.05). In Eμ-myc mice, ^{99m}Tc-C2Am detected baseline levels of cell death in cervical tumors (Fig. 6A, left panel) and there was a ∼1.9× increase (P<0.0001) in tumor signal post treatment (Fig. 6B, upper panel). Both cervical (Fig. 6A, ①) and axillary (Fig. 6A, ②) node tumors were clearly visible (Fig. 6A, arrow heads) following treatment (see Supplemental video 1). Histological analysis of tumor sections showed a similar increase in tumor cell death post treatment (~3×; P<0.05) (Fig. 6B, lower panel). In EL4 tumors ^{99m}Tc-C2Am uptake increased post-treatment by ∼1.3× (P<0.05), paralleling the modest increase and reflecting the wide variation in the levels of

8

cell death in this tumor model (~1.6×; P<0.05). Treatment response was also observed in the spleen and salivary glands of these etoposide-treated animals (Supplemental Fig. 4 and Supplemental video 1).

DISCUSSION

Phosphatidylserine exposed by dying cells constitutes a temporally stable and abundant biomarker for detection of cell death (*23*). We have been developing the C2Am domain of Synaptotagmin-I, which binds phosphatidylserine with nanomolar affinity, as a cell death imaging agent (*16*). Previous work with mouse lymphoma (EL4) and human triple-negative breast cancer (MDA-MB-231) cells demonstrated that C2Am has a higher specificity for binding to dead and dying cells *in vitro*, when compared with AnxV (*16*). We have demonstrated here, *in vivo*, that ^{99m}Tc-C2Am and ^{111}In-C2Am have favorable biodistribution profiles with predominantly renal clearance (Table 1, Supplemental Fig. 4), and that C2Am was capable of detecting cell death *in vivo* with high sensitivity and specificity, in three mouse models, from as early as 2 h post administration.

Binding of C2Am-AF750 was closely correlated with tumor cell death (Figs. 1−3), detecting cell death in regions with levels of CC3 staining as low as ~2% (Fig. 2B, lower panel; Figs. 3A & 3C, right panels). Although iC2Am-AF750 showed a small increase in uptake in EL4 tumors following treatment (Fig. 2A, upper panel), this likely reflects an increased EPR effect following treatment (*24*). This effect was not observed in the other two tumor models, Eμ-myc and Colo-205 (Fig. 2B & 2C, upper panels), possibly due to lower levels of cell death in these models leading to better clearance of the probe from the tumor.

[111]In-C2Am detected a treatment response in Colo-205 tumors within 2 h of probe administration, where the 60% increase in probe retention in treated tumors paralleled the increase in cell death determined histologically in tumor sections obtained post mortem, from 1.59±0.17% to 2.62±0.48% (Fig. 5B, P<0.05). In Eμ-myc tumors treatment resulted in a greater proportional increase in cell death (3×) and consequently a greater increase in

9

^{99m}Tc-C2Am retention (1.9×) (Fig. 6). In EL4 tumors, despite high levels of pre-existing cell death and a modest increase post treatment (1.6×) (Supplemental Fig. 4B), ^{99m}Tc-C2Am was nevertheless able to detect a significant treatment response (1.3× increase in probe retention, P<0.05, Supplemental Fig. 4B). The capability of C2Am to detect small percentage increases in cell death suggests that C2Am should be capable of detecting treatment response in the clinic. For example, levels of cell death can range from <2% prior to treatment to 5−15% post treatment (25). These data also suggest that C2Am would be effective clinically in those tumors that show high levels of pre-existing cell death, such as non-Hodgkin lymphoma, where high levels of spontaneous cell death (necrosis) have been reported in 25% of patients, frequently correlating with advanced disease and poor prognosis (26). Increased uptake of ^{99m}Tc-C2Am was also observed in the spleen and salivary glands of etoposide-treated animals (Fig. 4B, Supplemental Fig. 4A) and can be explained by etoposide-induced cell death in these tissues (27-28).

Several imaging agents have been developed to detect tumor cell death, some of which have progressed to the clinic. Annexin-V (AnxV) binds phosphatidylserine with high affinity (5) and has been used widely as a preclinical tool for detecting cell death, both *in vitro* and *in vivo*. However, binding of AnxV to tumor tissue following therapy is thought not to be entirely phosphatidylserine-specific, possibly explaining the limited success of AnxV in the clinic, which has been hampered by high levels of non-specific binding to viable tissues, including the liver, gut and kidneys (29). Modifications to AnxV have shown limited improvements in biodistribution or contrast agent performance *in vivo* (8). Duramycin is a 19-amino acid peptide that binds with high affinity and specificity to the phosphatidylethanolamine externalized by dying cells (30). ^{99m}Tc-labeled duramycin has been used recently to detect response to chemotherapy in a mouse model of colorectal cancer, where accumulation of the agent was found to correlate with markers of cell death (31). However, the clinical utility of duramycin has yet to be demonstrated. Imaging agents that target cleaved and activated caspase-3 (CC3), an executioner caspase in the apoptosis pathway, have also been developed for detection of cell death *in vivo* (25) and a probe capable of detecting CC3 has progressed to clinical trials (32). However,

10

since CC3 is a transient biomarker of cell death, the choice of temporal imaging window following treatment is critical (*33*). Furthermore CC3-targeted imaging agents are unable to identify caspase-independent modes of cell death, such as necrosis (*34*), which is often present following chemo or radiotherapy. ^{18}F-ML-10, which appears to bind to dead cells by an unknown mechanism, has shown favorable safety and biodistribution profiles in humans (*35*). In a clinical study in ten patients with brain metastasis, there was enhanced retention (up to 2-fold) of ^{18}F-ML-10 post radiotherapy and a good correlation between probe uptake and tumor size reduction (*36*). However, there was no histological demonstration of increased cell death and the average reported decrease in tumor size post therapy was substantial (ca. 60% reduction). Therefore, the utility of ^{18}F-ML-10 for detecting cell death in the most common clinical scenarios, in which therapy induces low levels of tumor cell death, has yet to be demonstrated.

CONCLUSION

We have demonstrated the capability of C2Am to detect tumor cell death *in vivo* as early as 2 h after administration. Radiolabelled C2Am derivatives showed favorable biodistribution profiles, with predominantly renal clearance and there was a close correlation between C2Am binding and histological markers of cell death. The capability of C2Am to detect relatively modest increases in cell death suggests that these agents will have sufficient sensitivity to detect tumor cell death in the clinic,

DISCLOSURE

11

REFERENCES

1. Eisenhauer EA, Therasse P, Bogaerts J, et al. New response evaluation criteria in solid tumours: revised RECIST guideline (version 1.1). *Eur J Cancer*. 2009;45:228-247.

2. Brindle K. New approaches for imaging tumour responses to treatment. *Nat Rev Cancer*. 2008;8:94-107.

3. Neves AA, Brindle KM. Imaging cell death. *J Nucl Med*. 2014;55:1-4.

4. Dean E, Greystoke A, Ranson M, Dive C. Biomarkers of cell death applicable to early clinical trials. *Exp Cell Res*. 2012;318:1252-1259.

5. Kuge Y, Zhao S, Takei T, Tamaki N. Molecular imaging of apoptosis with radio-labeled Annexin A5 focused on the evaluation of tumor response to chemotherapy. *Anticancer Agents Med Chem*. 2009;9:1003-1011.

6. Belhocine T, Steinmetz N, Hustinx R, et al. Increased uptake of the apoptosis-imaging agent (99m)Tc recombinant human Annexin V in human tumors after one course of chemotherapy as a predictor of tumor response and patient prognosis. *Clin Cancer Res*. 2002;8:2766-2774.

7. Hoebers FJ, Kartachova M, de Bois J, et al. 99mTc Hynic-rh-Annexin V scintigraphy for in vivo imaging of apoptosis in patients with head and neck cancer treated with chemoradiotherapy. *Eur J Nucl Med Mol Imaging*. 2008;35:509-518.

8. Bauwens M, De Saint-Hubert M, Devos E, et al. Site-specific 68Ga-labeled Annexin A5 as a PET imaging agent for apoptosis. *Nucl Med Biol*. 2011;38:381-392.

9. Kartachova MS, Verheij M, van Eck BL, Hoefnagel CA, Olmos RA. Radionuclide imaging of apoptosis in malignancies: promise and pitfalls of Tc-Hynic-rh-Annexin V imaging. *Clin Med Oncol*. 2008;2:319-325.

10. De Saint-Hubert M, Mottaghy FM, Vunckx K, et al. Site-specific labeling of 'second generation' annexin V with 99mTc(CO)3 for improved imaging of apoptosis in vivo. *Bioorganic Med Chem*. 2010;18:1356-1363.

11. Zhao M, Beauregard DA, Loizou L, Davletov B, Brindle KM. Non-invasive detection of apoptosis using magnetic resonance imaging and a targeted contrast agent. *Nat Med*. 2001;7:1241-1244.

12. Krishnan AS, Neves AA, de Backer MM, et al. Detection of cell death in tumors by using MR imaging and a gadolinium-based targeted contrast agent. *Radiology*. 2008;246:854-862.

13. Wang F, Fang W, Zhao M, et al. Imaging paclitaxel (chemotherapy)-induced tumor apoptosis with 99mTc C2A, a domain of Synaptotagmin I: a preliminary study. *Nucl Med Biol*. 2008;35:359-364.

14. Fang W, Wang F, Ji S, et al. SPECT imaging of myocardial infarction using 99mTc-labeled C2A domain of synaptotagmin I in a porcine ischemia-reperfusion model. *Nucl Med Biol*. 2007;34:917-923.

15. Wang F, Fang W, Zhang MR, et al. Evaluation of chemotherapy response in VX2 rabbit lung cancer with 18F-labeled C2A domain of synaptotagmin I. *J Nucl Med*. 2011;52:592-599.

16. Alam IS, Neves AA, Witney TH, Boren J, Brindle KM. Comparison of the C2A domain of Synaptotagmin-I and Annexin-V as probes for detecting cell death.

13

Bioconjug Chem. 2010;21:884-891.

17. Davies BR, Logie A, McKay JS, et al. AZD6244 (ARRY-142886), a potent inhibitor of mitogen-activated protein kinase/extracellular signal-regulated kinase kinase 1/2 kinases: mechanism of action in vivo, pharmacokinetic/pharmacodynamic relationship, and potential for combination in preclinical models. *Mol Cancer Ther*. 2007;6:2209-2219.

18. Harris AW, Pinkert CA, Crawford M, Langdon WY, Brinster RL, Adams JM. The E mu-myc transgenic mouse. A model for high-incidence spontaneous lymphoma and leukemia of early B cells. *J Exp Med*. 1988;167:353-371.

19. Workman P, Aboagye EO, Balkwill F, et al. Guidelines for the welfare and use of animals in cancer research. *Br J Cancer*. 2010;102:1555-1577.

20. von Poser C, Ichtchenko K, Shao X, Rizo J, Sudhof TC. The evolutionary pressure to inactivate. A subclass of synaptotagmins with an amino acid substitution that abolishes Ca2+ binding. *J Biol Chem*. 1997;272:14314-14319.

21. Blankenberg FG, Vanderheyden J-L, Strauss HW, Tait JF. Radiolabeling of HYNIC-annexin V with technetium-99m for in vivo imaging of apoptosis. *Nat Protoc*. 2006;1:108-110.

22. Maeda H, Nakamura H, Fang J. The EPR effect for macromolecular drug delivery to solid tumors: Improvement of tumor uptake, lowering of systemic toxicity, and distinct tumor imaging in vivo. *Adv Drug Deliv Rev*. 2013;65:71-79.

23. Martin SJ, Reutelingsperger CP, McGahon AJ, et al. Early redistribution of plasma membrane phosphatidylserine is a general feature of apoptosis regardless of the initiating stimulus: inhibition by overexpression of Bcl-2 and Abl. *J Exp Med*. 1995;182:1545-1556.

24. Maeda H, Wu J, Sawa T, Matsumura Y, Hori K. Tumor vascular permeability and the EPR effect in macromolecular therapeutics: A review. *J Control Release*. 2000;65:271-284.

25. Nguyen QD, Smith G, Glaser M, Perumal M, Arstad E, Aboagye EO. Positron emission tomography imaging of drug-induced tumor apoptosis with a caspase-3/7 specific [18F]-labeled isatin sulfonamide. *Proc Natl Acad Sci U S A*. 2009;106:16375-16380.

26. Saito A, Takashima S, Takayama F, Kawakami S, Momose M, Matsushita T. Spontaneous extensive necrosis in non-Hodgkin lymphoma: prevalence and clinical significance. *J Comput Assist Tomogr*. 2001;25:482-486.

27. Sefc L, Psenak O, Sykora V, Sulc K, Necas E. Response of hematopoiesis to cyclophosphamide follows highly specific patterns in bone marrow and spleen. *J Hematother Stem Cell Res*. 2003;12:47-61.

28. Anderson SM, Reyland ME, Hunter S, Deisher LM, Barzen KA, Quissell DO. Etoposide-induced activation of c-jun N-terminal kinase (JNK) correlates with drug-induced apoptosis in salivary gland acinar cells. *Cell Death Differ*. 1999;6:454-462.

29. Kurihara H, Yang DJ, Cristofanilli M, et al. Imaging and dosimetry of 99mTc EC Annexin V: preliminary clinical study targeting apoptosis in breast tumors. *Appl Radiat Isot*. 2008;66:1175-1182.

30. Zhao M. Lantibiotics as probes for phosphatidylethanolamine. *Amino Acids*. 2011;41:1071-1079.

31. Elvas F, Vangestel C, Rapic S, et al. Characterization of [(99m)Tc]Duramycin as a SPECT Imaging Agent for Early Assessment of Tumor Apoptosis. *Mol Imaging Biol*. 2015;17:838-847.

32. Challapalli A, Kenny LM, Hallett WA, et al. 18F-ICMT-11, a caspase-3-specific PET tracer for apoptosis: biodistribution and radiation dosimetry. *J Nucl Med*. 2013;54:1551-1556.

33. Reshef A, Shirvan A, Akselrod-Ballin A, Wall A, Ziv I. Small-molecule biomarkers for clinical PET imaging of apoptosis. *J Nucl Med*. 2010;51:837-840.

34. Witney TH, Fortt RR, Aboagye EO. Preclinical assessment of carboplatin treatment efficacy in lung cancer by 18F-ICMT-11-positron emission tomography. *PLoS One*. 2014;9:e91694.

35. Hoglund J, Shirvan A, Antoni G, et al. F-18-ML-10, a PET tracer for apoptosis: first human study. *J Nucl Med*. 2011;52:720-725.

36. Allen AM, Ben-Ami M, Reshef A, et al. Assessment of response of brain metastases to radiotherapy by PET imaging of apoptosis with (1)(8)F-ML-10. *Eur J Nucl Med Mol Imaging*. 2012;39:1400-1408.
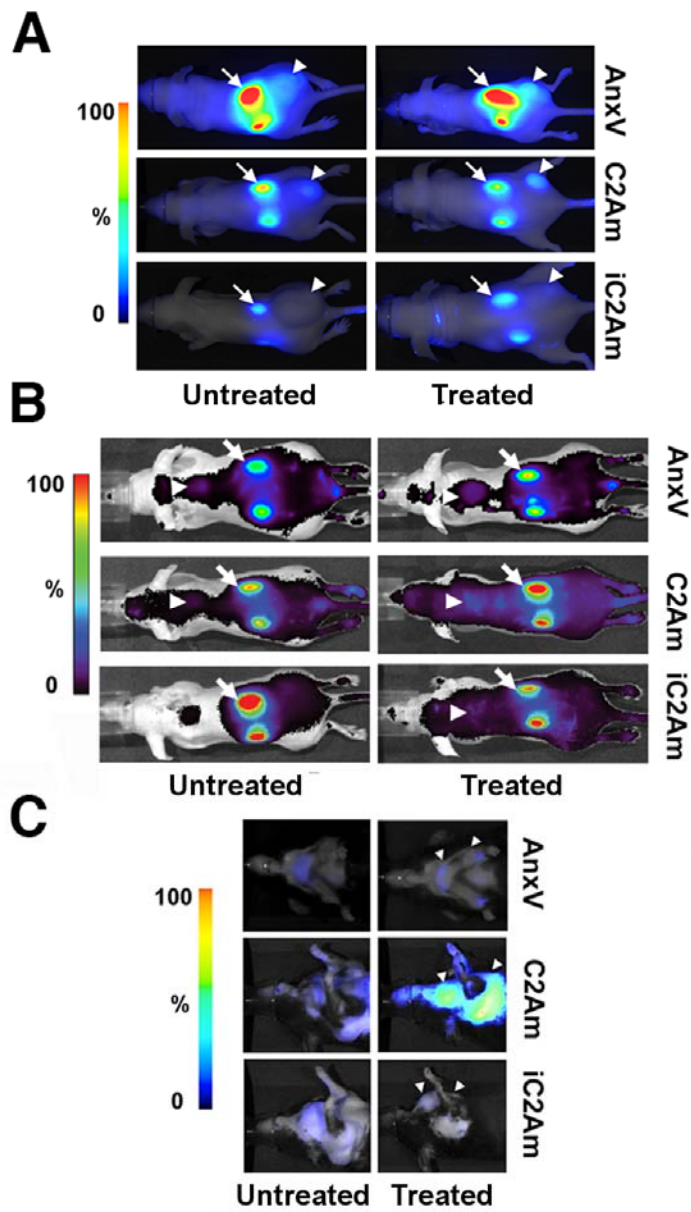
15

FIGURE 1. Near Infrared Fluorescence (NIRF) imaging of cell death. Imaging *in vivo* of untreated and treated EL4 (A), Colo-205 (B) and Eμ-myc (C) tumors.   Images are overlays of bright-field images and 800 nm-channel fluorescence signals, acquired 24 h after C2Am-AF750 administration.
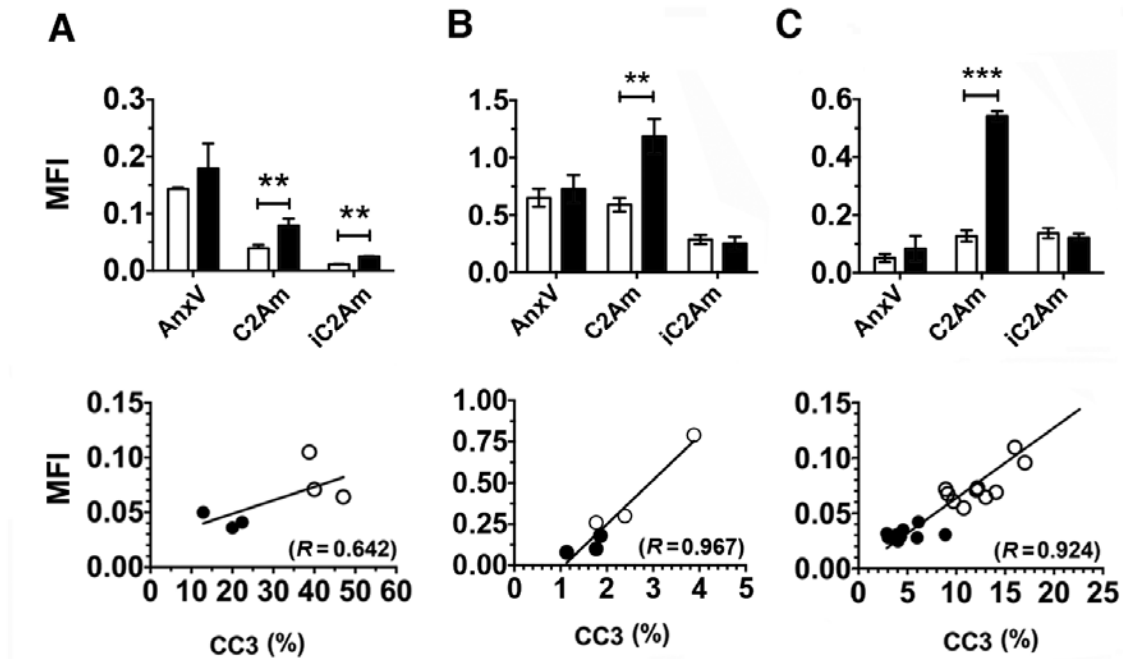
FIGURE 2. NIRF imaging of cell death. Tumor mean fluorescence intensity (MFI) for untreated (open bars) and treated (filled bars) EL4 (A), Colo-205 (B) and Eμ-myc (C) tumors. Data for the Eμ-myc model was acquired *ex vivo*, due to skin pigmentation artifacts. Lower panels show correlation of C2Am whole tumor MFIs with corresponding cleaved caspase-3 (CC3) staining, measured in sections of excised EL4 (A), Colo-205 (B) and Eμ-myc (C) tumors. Drug-treated (open circles, 48 h post treatment) and untreated (filled circles). **P<0.01, ***P<0.001, n=3/group, values are mean ± SD.
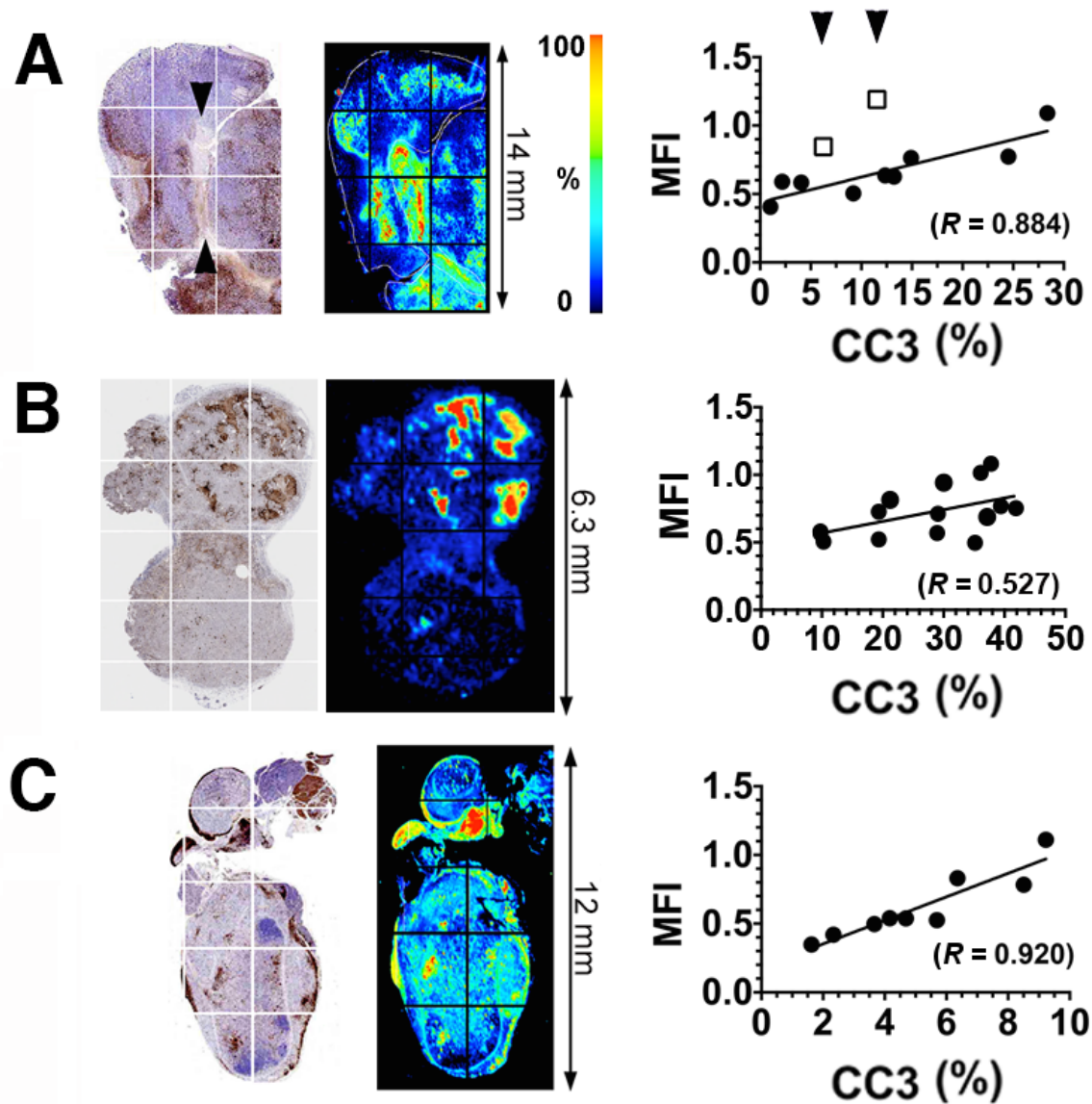
FIGURE 3. Maps of CC3 staining (left column), C2Am-AF750 fluorescence (middle column), and correlation (right column) of fluorescence intensities of regions of interest (ROIs; grids indicated in the left column), with staining for CC3 in the same ROIs. Tumors were excised 24 h after C2Am-AF750 administration and 48 h after drug treatment. The correlation coefficients (R) of the linear fits to the data (A-C, right column) are shown. Arrows in A (left column) indicate decellularized regions of tissue. Sections from EL4 (A), Colo-205 (B) and Eμ-myc (C) tumors.
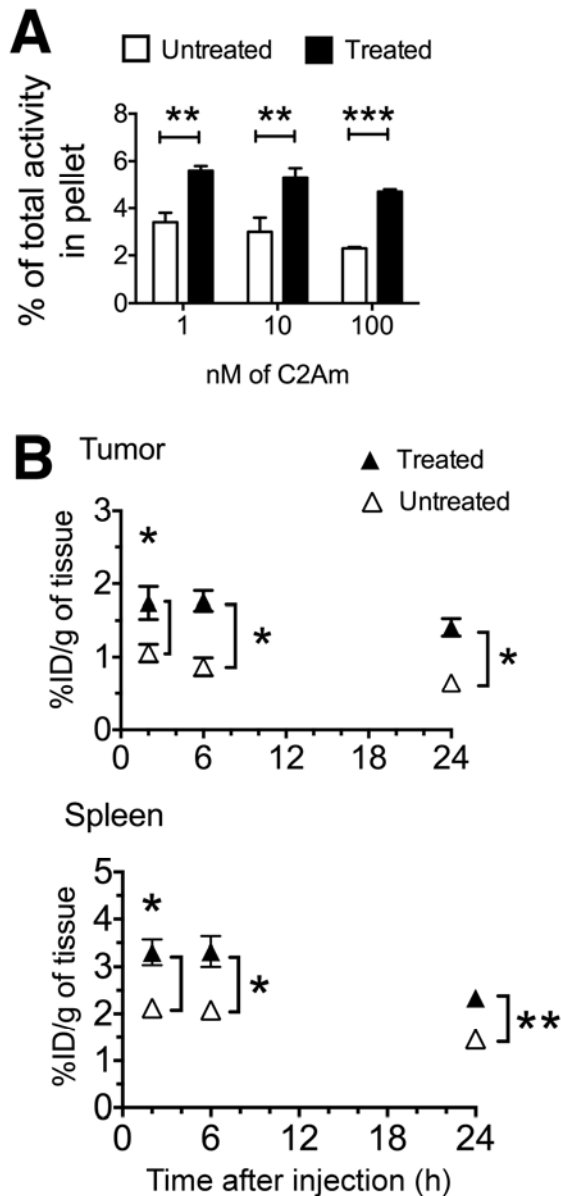
18

FIGURE 4. (A) Binding of ^{99m}Tc-C2Am to EL4 cells. Labeling of drug-treated and untreated cells is expressed as a percentage of the total ^{99m}Tc activity retained by the cell pellets. **P<0.01, ***P<0.001, n=3/group, values are mean ± SD. (B) Retention of ^{99m}Tc-C2Am in tumors (top panel) and spleens (lower panel) from EL4 tumor-bearing mice, in untreated (△) and drug-treated (▲) animals, at the indicated times after probe administration. Tissue retention is expressed as % of injected dose per gram of tissue (%ID/g of tissue). *P<0.05, n=3/group, 2-way analysis of variance, with Bonferroni post-test correction, was used for group comparisons. Values are mean ± SD.

19

FIGURE 5. SPECT imaging of cell death *in vivo* in Colo-205 tumors. Imaging of ^{111}In-labeled C2Am was performed 2 h after probe administration, and 24 h after drug treatment. (A) SPECT-CT fusion images of a representative untreated Colo-205 tumor-bearing mouse (A, left panel) and a 5-FU treated animal (A, right panel), 2 h post administration of ^{111}In-C2Am (A). Tumor location is indicated by the arrowheads. (B) Tumor retention (% ID/mL) (upper panel) and CC3 staining (lower panel) in untreated and 5-FU-treated tumors. *P<0.05, n=3−4 tumors/group (B).
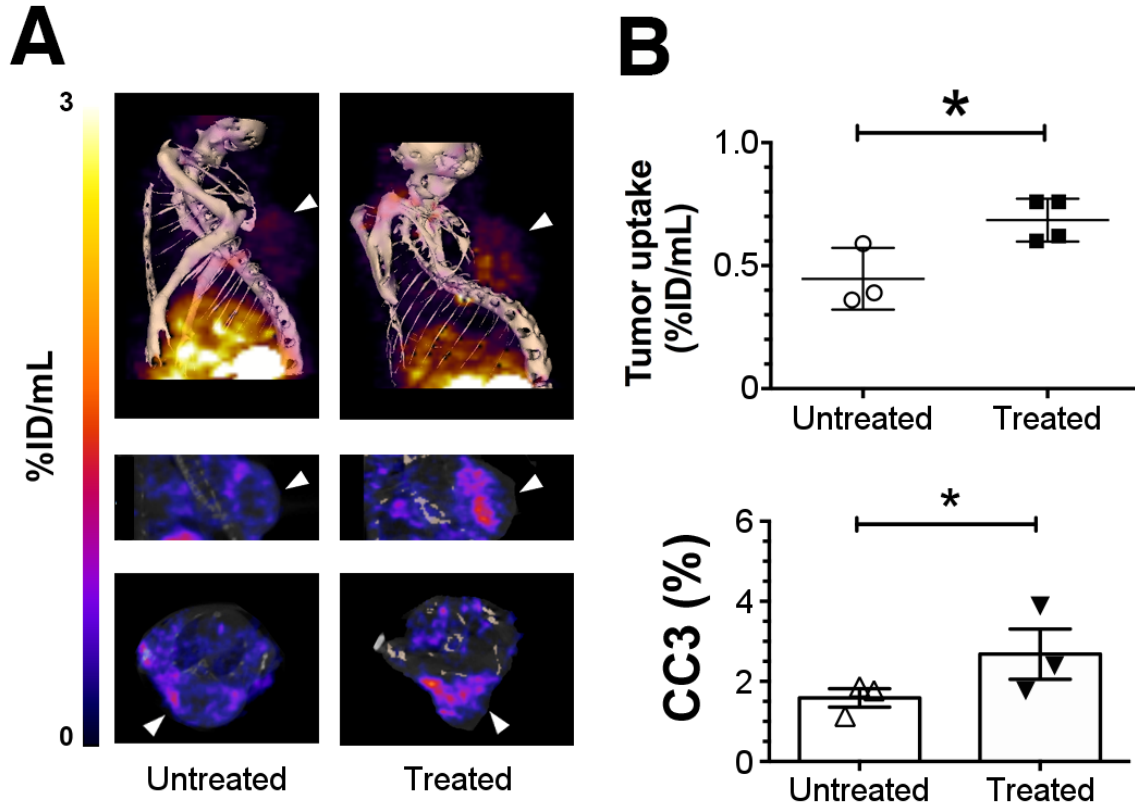
FIGURE 6. SPECT imaging of cell death *in vivo* in Eμ-myc tumors. Imaging of ^{99m}Tc-labeled C2Am was performed 2 h after probe administration, and 24 h after drug treatment. (A) SPECT-CT fusion images of representative Eμ-myc mice before (left) and after (right) cyclophosphamide treatment. Tumors in the neck, axillary region and chest cavity were visible (arrowheads, upper panel) and in axial sections across cervical (①, middle panel) and axillary (②, lower panel) planes. The red circles in (B) correspond to the %ID/mL retention values for tumors of the animals shown in (A). CC3 staining (B, lower panel) in untreated and drug-treated tumors. *P<0.05, ***P<0.0001, n=6−7 tumors/group (A); n=6−13 tumors/group (B). Abbreviations: BT, AT, before and after treatment, respectively. See Supplemental Data for statistical analysis. 3D rendering of the SPECT data are shown in Supplemental video 1.

21

Table 1 – Biodistribution of ^{99m}Tc-C2Am in tumor-bearing EL4 mice (A) and of ^{111}In-C2Am in tumor-bearing Colo-205 mice (B), 24 h after etoposide and 5-FU treatment respectively and at the indicated times after probe administration. n=3/group.

Tissue	2 hours		24 hours	
(%ID/g)	Mean	SD	Mean	SD
A				
Muscle	0.39	0.05	0.19	0.02
Blood	1.02	0.08	0.20	0.01
Tumor	1.74	0.39	1.41	0.21
Spleen	3.30	0.47	2.34	0.29
Liver	6.17	0.98	5.14	0.90
Kidney	194.2	45.9	157.4	57.0
Tumor-to-blood	1.71	0.40	6.96	1.08
Tumor-to-muscle	4.5	1.15	7.3	1.40
B	**Mean**	**SD**	**Mean**	**SD**
Muscle	0.32	0.07	0.18	0.02
Blood	0.50	0.22	0.13	0.02
Tumour	0.69	0.09	0.72	0.10
Spleen	0.92	0.17	1.18	0.20
Liver	2.01	0.34	2.17	0.53
Kidney	310	12	275	22
Tumour-to-blood	1.38	0.65	5.43	0.96
Tumour-to-muscle	2.16	0.48	4.09	0.88

Rapid Imaging of Tumor Cell Death *in vivo* using

the C2A domain of Synaptotagmin-I

Files in this Data Supplement:

Supplemental Methods,

Supplemental Figures 1, 2, 3 & 4,

Supplemental Table 1 & 2,

Supplemental References -

Supplemental Figure 1. Analysis of imaging probes using electrospray ionization mass spectrometry (ESI-MS).

Supplemental Figure 2. Analysis of ^{99m}Tc and ^{111}In labeling of C2Am using gel filtration radio-HPLC.

Supplemental Figure 3. Splenic response to etoposide treatment.

Supplemental Figure 4. SPECT imaging of cell death *in vivo* in EL4 tumors.

Supplemental Table 1. Surface Plasmon Resonance (SPR) analysis of imaging probes.
Supplemental Table 2. Biodistribution of NIRF labeled C2Am-AF750 and iC2Am-AF750.

Supplemental Methods

Probe expression and chemical labeling

iC2Am (D108N) was produced using a QuickChange Site-Directed Mutagenesis kit (Stratagene). C2Am was labeled with hydrazinonicotinic acid (HYNIC) using methods similar to those used for fluorophore labeling. Briefly, an aliquot of the protein (1 mg/mL) was reduced in HEPES-buffered saline (HBS buffer: 20 mM HEPES, 150 mM NaCl, pH 7.4) containing 10 mM dithiothreitol (DTT) at room temperature for 30 min. The reduced protein was then washed with ice cold HBS in a 5-kDa Vivaspin™ (Sartorius) and concentrated to 1 mg/mL, prior to the addition of maleimide-HYNIC (Solulink) at a 5-fold molar excess in DMSO. Reaction was conducted at room temperature for 1 h with stirring (200 r.p.m) and quenched by addition of glycine (0.6M, pH 9.2) to 0.05 M. A similar method was used to conjugate C2Am to maleimide-DOTA (Macrocyclics B-272).

Active (C2Am) and inactive (iC2Am) forms of C2Am-AF750 were prepared using Alexa-Fluor®750 C5-maleimide (AF750, Invitrogen™, λexc=750 nm, λem=775 nm), following the method described in (*1*). Briefly, the protein was reduced in HBS buffer containing 10 mM DTT, for ½ h at room temperature. The protein was then washed in a 5-kDa Vivaspin concentrator in HNE buffer (20 mM, HEPES, 100 mM NaCl, 5 mM EDTA, pH 7.4). The protein was used at a concentration in the range 50-100 μM, and an approximately 10-fold molar excess of the fluorescent maleimide dye was added to the reaction mixture. The reaction was allowed to proceed at 4 °C for 16 h. The modified protein was separated from unreacted dye by gel filtration using a Hi-Load Superdex 75 26/60 preparation grade column (GE Healthcare, Amersham, UK).

Probe radiolabeling with ^{99m}Tc

C2Am-HYNIC was labeled with ^{99m}-Tc pertechnetate (^{99m}Tc-C2Am), eluted from an Ultra-Technekow™ DTE (Covidien) and supplied at 1.5-2.0 GBq/mL by the Department of Nuclear Medicine (Cambridge University Hospitals), as described previously (*2*). To 50 µL of C2Am-HYNIC (715 nmol in 115 mM tricine buffer, pH 6±1), 200 µL of 0.9% degassed saline were added, followed by 20 µL of pertechnetate (ca. 40 MBq) and 20 µL of degassed stannous tricine solution (0.17 mg/mL $SnCl_2$, 6.7 mg/mL tricine and 0.9% NaCl) and the reaction allowed to proceed at room temperature for 10 min.

Probe radiolabeling with [111]In

C2Am-DOTA (60 μg; 20 µL) was labeled by adding 20 µL of acetate buffer 0.2 M pH 5.5, 8 µL 1 M pH 5.5 and 40-50 µL (30–40 MBq) of high purity [111]InCl$_3$ (supplied at 0.8-1 GBq/mL by the Department of Nuclear Medicine, Cambridge University Hospitals) at 37 °C for 30 min, with orbital shaking (600 r.p.m.). Free ^{111}In was removed using a 5-kDa cut-off spin Amicon-ultra filter (Millipore).

All C2Am conjugates were washed and concentrated using Vivapsin concentrators and analyzed by Electrospray Ionization Mass Spectrometry (ESI-MS) (*1*) (Supplemental Figure 1).

Cell binding assays using ^{99m}Tc-C2Am

Etoposide-treated (15 µM, 24 h) or untreated EL4 cells were washed in ice-cold HBS[+] buffer (HBS with 2 mM CaCl$_2$), pelleted (600g, 4°C, 4min), and re-suspended in the same buffer at $1x10^7$ cells/mL, incubated with ^{99m}Tc-C2Am (1-100 nM), at 37 °C for 30 min in an orbital shaker (250 r.p.m.). The cells were then washed in cold HBS[+] buffer 3 times, prior to measurement of radioactivity in the cell pellets (ISOMED 2100 well counter, MED Nuklear-Medisintechnik GmbH).

SPECT studies

A NanoSPECT system (Bioscan Inc.) with 4 detector heads (230×215 mm; sodium iodide crystals) with multiple pinholes (36×2.0mm) was used. A minimum of 50,000 counts/projection were collected and the data reconstructed to give an isotropic resolution of 300 μm. CT images were acquired by helical acquisition using a microtomography system (NanoPET/CT, Mediso) and reconstructed using a modified cone beam filtered back projection method using a Butterworth filter to give an isotropic resolution of 212 μm. SPECT and CT images were fused and radioactivity quantified using VivoQuant [TM] 1.22 (InviCRO), and rendered in 3D for detailed visualization.

Immunohistochemistry and *ex vivo* imaging of tissue fluorescence

Excised tissues were weighed, radioactivity measured as described above and approximately half of each specimen was placed in 10% neutral buffered formalin (NBF, 10%, Acquascience). Unstained tissue sections were de-waxed and rehydrated and slides mounted using Prolong Gold™ antifade reagent (Life Technologies), cured for 24 h at room temperature, prior to microscopic NIRF imaging
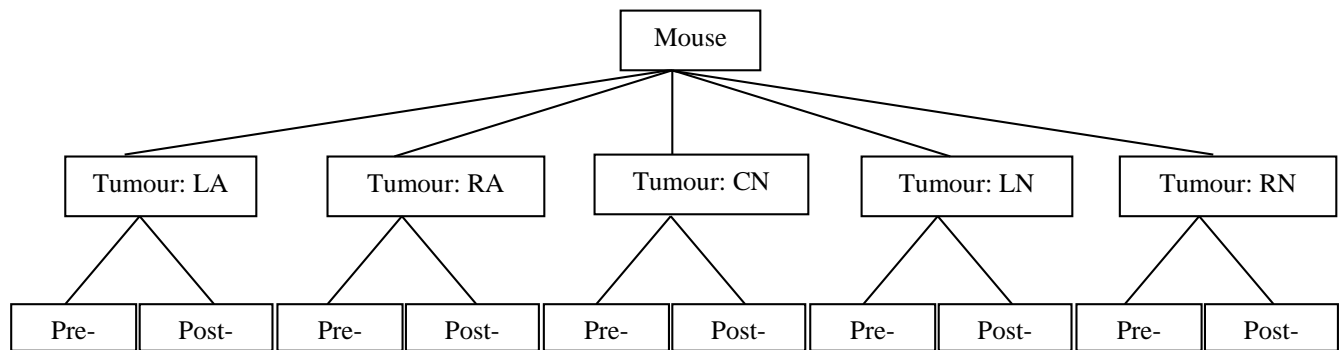
at a resolution of 21 μm, using a Odyssey™ (Li-Cor) flat-bed scanner. Tissues fixed for 24 h in NBF were transferred into 70% ethanol and sections (3-μm) cut using a rotary microtome. Hematoxylin and eosin (H&E) staining was performed on a Leica ST5020/CV5030 workstation (Leica Biosystems). For cleaved-caspase-3 (CC3) staining, a rabbit monoclonal anti-CC3 antibody (Cell Signaling Technology™ Inc., used at a 1:100 dilution) and a donkey anti-rabbit secondary biotinylated antibody (Jackson ImmunoResearch Laboratories Inc., diluted 1:250 in Bond™ diluent) were used with a Leica Microsystems Bond™-Max (Leica Biosystems) system using a LM Bond™ Intense-R Detection Kit, which is based on streptavidin-horse-radish-peroxidase for detection of the secondary antibody. An avidin-biotin blocking kit was used (Vector Laboratories Inc). A hematoxylin nuclei counterstain was used. A Zeiss Mirax™ Scan 150 (Carl Zeiss) with a 20× objective was used to digitize tissue images (at 0.369 μm/pixel), which were stored using a Spectrum™ digital pathology information database (Aperio™). Aperio's ImageScope™ software was used for image analysis.

Statistics

Data are expressed as mean ± SD, unless stated otherwise. Two-tailed Student T-test, with Tukey's post-hoc non-parametric correction, was used for pairwise comparisons. Two-way ANOVA with Bonferroni post-test correction was used for multi-parametric analysis (GraphPad Prism version 5, Sigma Software). $P<0.05$ was considered statistically significant. Statistical analysis of SPECT imaging data was performed by the Bioinformatics Core of the CRUK Cambridge Institute (see Supplemental Materials and Methods).

Statistical Analysis of SPECT data (Figure 6).

Some animals could only be imaged either before or after treatment. For this reason, a mixed statistical model was fitted to the data in Figures 6, the structure of which is shown below. There were 6 mice in total, one of which had only pre-dose data and one of which had only post-dose data.

```
                              ┌─────────┐
                              │  Mouse  │
                              └─────────┘
```

| Tumour: LA | Tumour: RA | Tumour: CN | Tumour: LN | Tumour: RN |

| Pre- | Post- | Pre- | Post- | Pre- | Post- | Pre- | Post- | Pre- | Post- |

LA, RA: left, right axillary tumors, respectively; CN, LN, RN: central, left, right cervical nodal tumors, respectively.

Fixed effects for dose, protein and the dose*protein interaction were considered. Random effects were fitted for dose nested within tumor nested within mouse. During the model building process, random effects were compared using restricted maximum likelihood (REML) and fixed effects were compared using maximum likelihood (ML). The final model was fitted using REML. The analysis was conducted in R software vs. 2.14.1, using the nlme package (version 3.1.102). The R output for the final model is given below.

In a mixed effect model, usually only the parameter estimates for the fixed effects are interpreted. The results of the fixed effects part of the model are given in Table A.

Table A Fixed effects

Parameter	Reference level	Estimate	Standard error	95% confidence interval	P-value
Intercept	-	0.218	0.065	0.09 to 0.35	0.0028
Protein	C2Am	0.127	0.098	-0.06 to 0.32	0.2628
Dose	Post-dose	0.034	0.043	-0.05 to 0.12	0.4398
Protein*Dose	C2Am, Post-dose	0.284	0.079	0.13 to 0.44	0.0022

The results in Table A can be interpreted as follows:

- The difference between the pre- and post-treatment stages is 0.318 (0.034+0.284) SUV units for C2Am.

Residual plots were used to check for normality of the model residuals and these were satisfactory.

Post-hoc tests were performed to compare pre- and post-treatment measurements for each protein separately. This part of the analysis was conducted in R 2.14.1, using the multcomp package (version 1.2.17). The results are given in Table B. The P-values were adjusted for multiple testing using a Bonferroni correction.

Table B *Post-hoc comparisons*

Comparison	Estimated difference	Standard error	95% confidence interval	Adjusted P-value
Pre- v post-treatment for C2Am	0.318	0.067	0.19 to 0.45	<0.0001

The difference between the pre- and post-treatment measurements was significant for C2Am.

R output for final model:

```
> #Final model
>
> m.final <- lme(Response ~ Protein + relevel(Dose,ref="Pre") + Protein*relevel(Dose,ref="Pre"),
random=~1|ID/Tumour/Dose, data=mydata, method="REML", na.action=na.omit)
> summary(m.final)
Linear mixed-effects model fit by REML
 Data: mydata
      AIC      BIC    logLik
  12.60281 27.23194 1.698597

Random effects:
 Formula: ~1 | ID
        (Intercept)
StdDev: 2.22047e-05

 Formula: ~1 | Tumour %in% ID
        (Intercept)
StdDev:   0.2247239

 Formula: ~1 | Dose %in% Tumour %in% ID
        (Intercept)    Residual
StdDev:   0.1165061 0.006787696

Fixed effects: Response ~ Protein + relevel(Dose, ref = "Pre") + Protein * relevel(Dose,     ref =
"Pre")
                                               Value  Std.Error DF  t-value p-value
(Intercept)                                0.21783215 0.06538123 24 3.331723  0.0028
ProteinC2A                                 0.12696367 0.09751878  4 1.301941  0.2628
relevel(Dose, ref = "Pre")Post             0.03366731 0.04261415 18 0.790050  0.4398
ProteinC2A:relevel(Dose, ref = "Pre")Post 0.28407845 0.07943183 18 3.576380  0.0022
 Correlation:
                                          (Intr) PrtC2A r(Dr="
ProteinC2A                                -0.670
relevel(Dose, ref = "Pre")Post            -0.326  0.218
ProteinC2A:relevel(Dose, ref = "Pre")Post  0.175 -0.407 -0.536

Standardized Within-Group Residuals:
        Min          Q1          Med           Q3          Max
-0.116832335 -0.011816817 -0.002297878  0.009583274  0.196308461

Number of Observations: 50
Number of Groups:
                    ID         Tumour %in% ID Dose %in% Tumour %in% ID
                     6                     30                       50
```
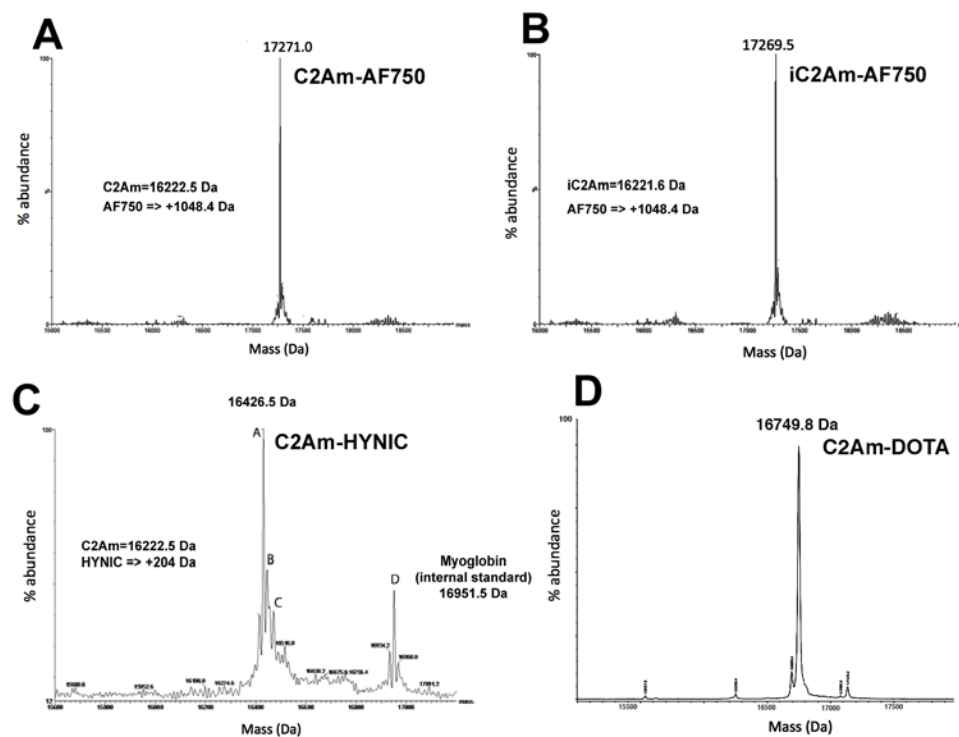
```
> anova(m.final)
                                    numDF denDF  F-value p-value
(Intercept)                            1    24 66.98628  <.0001
Protein                                1     4  9.12222  0.0392
relevel(Dose, ref = "Pre")             1    18 10.30247  0.0049
Protein:relevel(Dose, ref = "Pre")     1    18 12.79050  0.0022
```
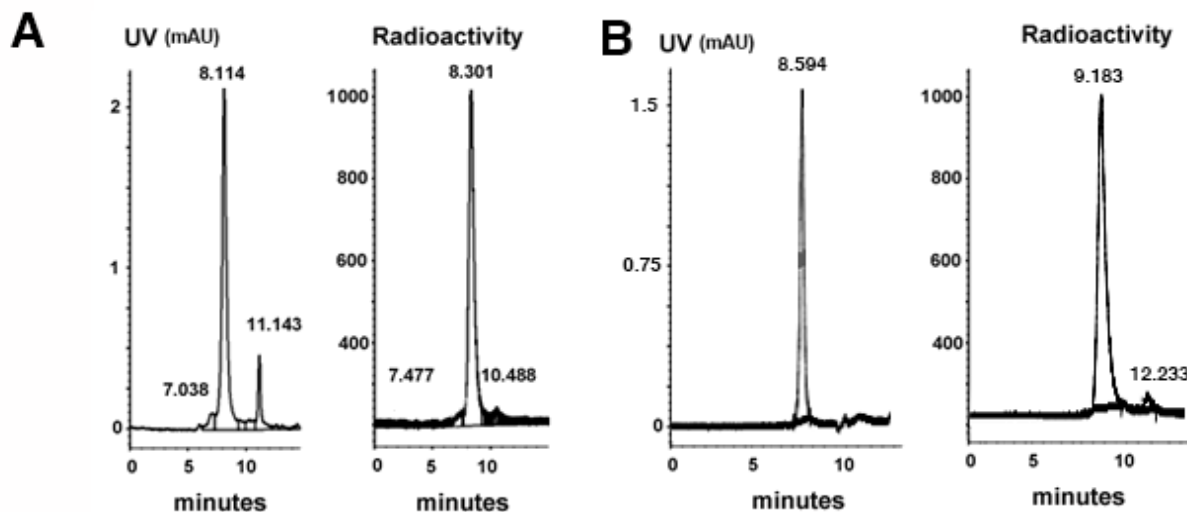

Supplemental Figure 1.

Analysis of imaging probes using electron spray ionization mass spectrometry (ESI-MS).

(A)   ESI spectrum of active C2Am-AF750 showed a single peak at 17271.0 Da, corresponding to the addition of one molecule of Alexa Fluor™ 750 (+1048.4 Da) to C2Am (16222.5 Da).

(B)   ESI spectrum of inactive-C2Am-AF750 (iC2Am-AF750) showed a single peak at 17269.5 Da, corresponding to the addition of one molecule of Alexa Fluor™ 750 to iC2Am (16221.6 Da).

(C)   Complete modification of C2Am with maleimido-HYNIC ligand to form C2Am-HYNIC (A). A heavier peak (B) is seen at 15 Da above (A) but is much smaller. Peak (D) represents myoglobin (16951.5 Da) added for calibration purposes. Note also the small heavier peak (C) (40 Da
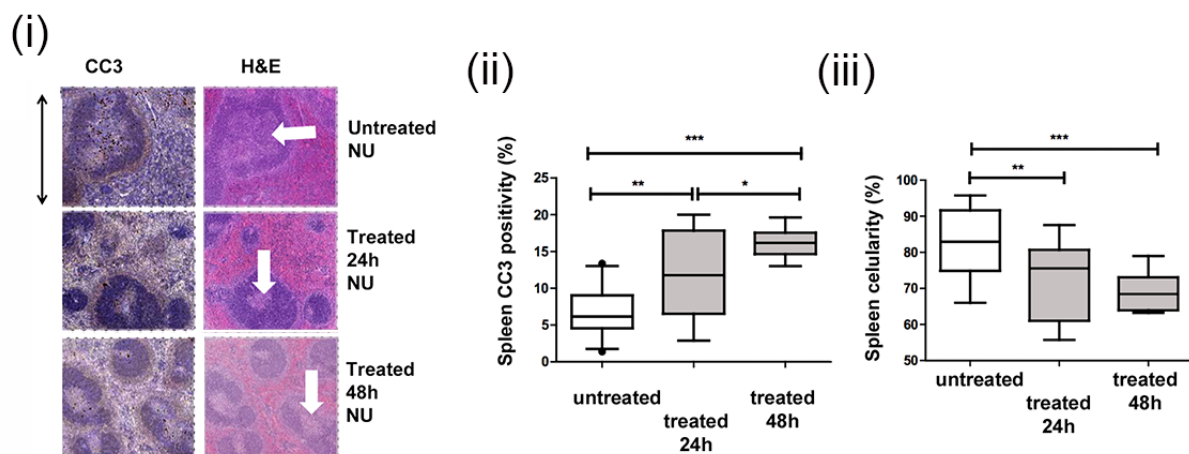
heavier than A), likely representing the K^+ bound form of C2Am-HYNIC.

(D)   Complete modification of C2Am with maleimido-DOTA to form C2Am-DOTA (16749.8 Da).

Supplemental Figure 2.

Analysis of ^{99m}Tc- and ^{111}In- labeling of C2Am using gel filtration radio-HPLC.

(A) ^{99m}Tc-C2Am-HYNIC, the dominant peak at 8.30 min in the radioactivity channel, was ^{99m}Tc-labeled C2Am, corresponding to 8.114 min in the UV channel. Another minor peak visible at 10.48 min in the radioactivity channel is likely to be reduced pertechnetate. Tricine was visible in the UV channel at 11.14 min. Labeling efficiency of ^{99m}Tc-labeled C2Am was 94%.

(B) ^{111}In-C2Am-DOTA, the main species at 9.183 min in the radioactivity channel, was ^{111}In-labeled C2Am, corresponding to 8.594 min in the UV channel. The minor peak visible at 12.233 min in the radioactivity channel is ^{111}InCl3. Labeling efficiency of ^{111}In -labeled C2Am was 97%.
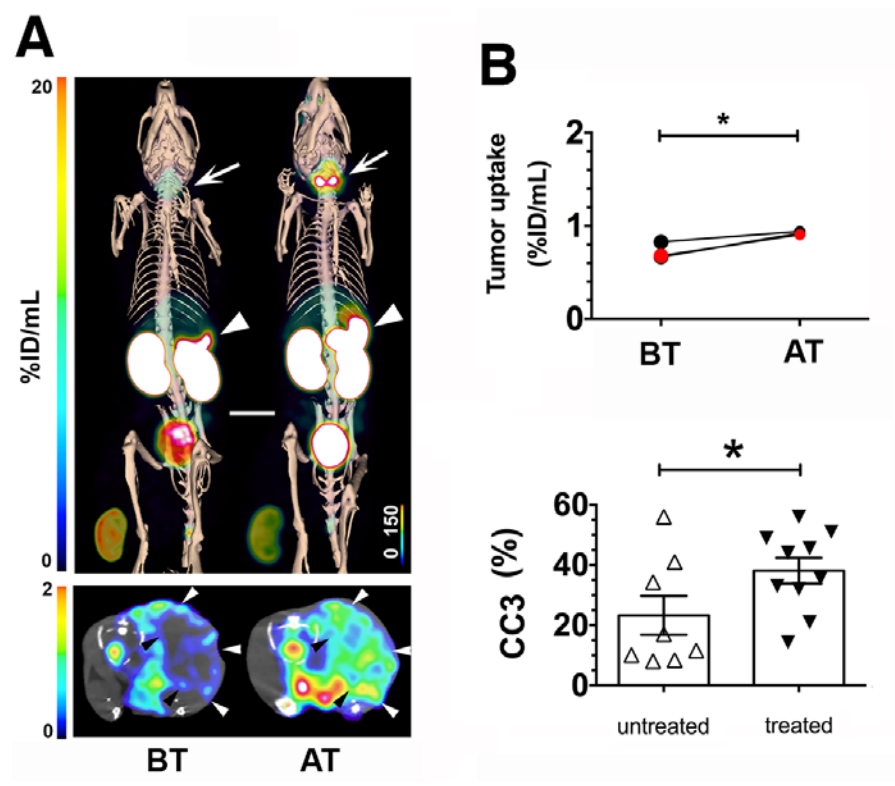
Supplemental Figure 3. Splenic response to etoposide treatment.

(i)　　H&E stained spleen sections in treated and untreated BalbC/NU animals.

(ii)　　Analysis of CC3 staining.

(iii)　　Spleen cellularity decreases with treatment.

Spleen sections (ii,iii) from untreated (n=20) or treated (n=10) mice were analyzed in each group. *P<0.05, **P<0.005, ***P<0.001, differences between groups (i, ii) were significant t-test.

Supplemental Figure 4.

SPECT imaging of cell death *in vivo* in EL4 tumors.

Imaging of ^{99m}Tc-labeled C2Am was performed 2 h after probe administration, and 26 h after drug treatment. (A) SPECT-CT fusion images of representative EL4 tumor-bearing mice before (A, left) and after (A, right) etoposide treatment and 2 h post administration of ^{99m}Tc-C2Am. Tumor location is indicated by the horizontal white line. The insets (top left) represent kidney signal on a larger vertical scale. ^{99m}Tc-C2Am accumulation in the salivary glands and spleen is indicated by the thin arrows and arrowheads. Arrowheads (A, lower) delineate tumor edges defined on CT. The red circles in (B) correspond to the %ID/mL values for the tumors of the animals shown in (A). (B, lower panel) CC3 staining in untreated and drug-treated tumors. *P<0.05, n=3 tumors/group (A), n=8-10 tumors/group (B). Abbreviations: BT, AT, before and after treatment, respectively. 3D rendering of SPECT data are shown in Supplemental video 1.

Supplemental Table 1. Surface Plasmon Resonance (SPR) analysis of imaging probes.

	kd (1/s)	ka (1/Ms)	KD (nM)	Rmax
iC2Am-AF750	N/D	N/D	N/D	N/D
C2Am-AF750	$3.89{\times}10^{-2}$ $\pm2{\times}10^{-4}$	$7.11{\times}10^{5}$ $\pm4.5{\times}10^{3}$	54.7 ±0.4	421.7 ±0.54
C2Am-HYNIC	$9.46{\times}10^{-2}$ $\pm1.3{\times}10^{-3}$	$1.392{\times}10^{6}$ $\pm2{\times}10^{4}$	68.0 ±1.4	505.9 ±1.2
C2Am-DOTA	$1.16{\times}10^{-2}$ $\pm1.1{\times}10^{-4}$	$1.299{\times}10^{5}$ $\pm1.4{\times}10^{3}$	89.3 ±0.2	469.8 ±9.3

Kinetic data analysis using Biacore T100 Evaluation 1.1.1 software. Concentration ranges 0-150 nM. Materials, methods and analysis were described previously (1). KD: thermal equilibrium dissociation constant (nM), ka, kd: kinetic association (1/Ms) and dissociation (1/s) constants, Rmax: maximum analyte binding capacity of the surface in response units (RU); values quoted are means $\pm$ standard deviation obtained from the fit to a 1:1 kinetic binding model. N/D-No detectable binding.

Supplemental Table 2 – Biodistribution of NIR-labelled imaging agents, in tumor-bearing EL4 mice, 24 h after etoposide treatment and at the indicated times after probe injection.

Tissue (TFI/mg)	2 hours		24 hours	
AnxV-AF750	Mean	SD	Mean	SD
Muscle	4.3	0.6	0.95	0.03
Spleen	7.7	0.8	2.68	0.25
Tumor	4.8	0.6	2.53	0.47
Liver	13.4	0.9	4.1	0.7
Kidney	88.9	5.6	60.0	5.0
Tumor-to-muscle	1.12	0.21	2.66	0.50
C2Am-AF750	Mean	SD	Mean	SD
Muscle	4.5	0.9	0.47	0.04
Spleen	3.6	0.4	0.63	0.02
Tumor	10.0	1.0	1.71	0.12
Liver	9.8	0.8	0.63	0.03
Kidney	161	6	38.6	1.1
Tumor-to-muscle	2.2	0.49	3.63	0.40
iC2Am-AF750	Mean	SD	Mean	SD
Muscle	6.1	1.8	0.32	0.02
Spleen	1.6	0.3	0.32	0.03
Tumor	4.9	0.3	0.35	0.02
Liver	4.1	0.2	0.3	0.03
Kidney	183	10	19.1	0.8
Tumor-to-muscle	0.80	0.24	1.1	0.1

TFI- total fluorescence intensity; data reported as TFI per mg of wet tissue mass, collected *post mortem*.

Supplemental References

1. Alam IS, Neves AA, Witney TH, Boren J, Brindle KM. Comparison of the C2A domain of Synaptotagmin-I and Annexin-V as probes for detecting cell death. *Bioconjug Chem*. 2010;21:884-891.

2. Blankenberg FG, Vanderheyden J-L, Strauss HW, Tait JF. Radiolabeling of HYNIC-annexin V with technetium-99m for in vivo imaging of apoptosis. *Nat Protoc*. 2006;1:108-110.

The Journal of NUCLEAR MEDICINE

Rapid Imaging of Tumor Cell Death in vivo using the C2A domain of Synaptotagmin-I

André A. Neves, Bangwen Xie, Sarah Fawcett, Israt S Alam, Timothy H Witney, Maaike M de Backer, Julia Summers, William Hughes, Sarah McGuire, Dmitry Soloviev, Jodie Miller, William J Howat, De-en Hu, Tiago B Rodrigues, David Y Lewis and Kevin M Brindle

This article and updated information are available at:
http://jnm.snmjournals.org/content/early/2017/02/15/jnumed.116.183004

Information about reproducing figures, tables, or other portions of this article can be found online at:
http://jnm.snmjournals.org/site/misc/permission.xhtml

Information about subscriptions to JNM can be found at:
http://jnm.snmjournals.org/site/subscriptions/online.xhtml

JNM ahead of print articles have been peer reviewed and accepted for publication in *JNM*. They have not been copyedited, nor have they appeared in a print or online issue of the journal. Once the accepted manuscripts appear in the *JNM* ahead of print area, they will be prepared for print and online publication, which includes copyediting, typesetting, proofreading, and author review. This process may lead to differences between the accepted version of the manuscript and the final, published version.

SNMMI
SOCIETY OF
NUCLEAR MEDICINE
AND MOLECULAR IMAGING